ISSN 1063-7710, Acoustical Physics, 2013, Vol. 59, No. 5, pp. 513–520. © Pleiades Publishing, Ltd., 2013.
Original Russian Text © M.Yu. Dvoesherstov, V.I. Cherednik, S.I. Bosov, I.Ya. Orlov, O.V. Rudenko, 2013, published in Akusticheskii Zhurnal, 2013, Vol. 59, No. 5, pp. 569–577.

PHYSICAL ACOUSTICS

Numerical and Experimental Analysis of the Parameters of an Electroacoustic Thin-Film Microwave Resonator

M. Yu. Dvoesherstov, V. I. Cherednik, S. I. Bosov, I. Ya. Orlov, and O. V. Rudenko

Nizhni Novgorod State University, pr. Gagarina 23, Nizhni Novgorod, 603950 Russia

e-mail: Dvoesh1@mail.ru

Received March 25, 2013

Abstract—The results of numerical and experimental analysis of the parameters of a single-frequency microwave thin-film electroacoustic resonator based on an (0001)AlN piezofilm with an acoustic reflector operating at a frequency of 10 GHz are presented. The effect of the reflector design on the resonator characteristics is considered. Using the modified Butterworth–Van Dyke model, it was shown that the ohmic resistance of electrodes and entrance paths substantially decreases the Q-factor at the resonance frequency of series and the acoustic losses in the resonator deteriorate the Q-factor at the parallel resonance frequency.

Keywords: simulation of wave processes, electroacoustic thin-film resonator, sensor

DOI: 10.1134/S1063771013050072

INTRODUCTION

There is currently a growing interest in thin-film electroacoustic microwave resonators of bulk acoustic waves (BAWs) and radio-engineering devices based on them (filters, duplexes). This is related to the fact that, as compared to analogous devices for acoustic waves of other types [1–8], the mass and dimensions of thin-film BAW resonators are smaller by an order of magnitude and they can operate at higher frequencies in the range of 2–12 GHz. At the same time, resonators of such type serve as a basis for developing sensors of physical and mechanical quantities and biosensor chips. The operating principle of such sensors is based on the superhigh sensitivity of the active resonator region to the parameters of the environment [9, 10]. Such sensors are primarily relevant in branches of medicine where timely and precise evaluation of the general state of a patient required for correct diagnosis and treatment is of particular significance. The key parameters of such sensors are their accuracy, dimensions, and the possibility of wireless instrument reading. This allows fabricating chip-based implants that allow monitoring the state of a patient over a long time period.

It is known [11, 12] that a single-frequency thin-film electroacoustic microwave resonator that operates for longitudinal BAWs consists of a thin piezofilm (e.g., (0001)AlN) with metal electrodes on its upper and lower surfaces. Acoustic insulation of the resonator from the substrate can be accomplished in two ways. The first method uses microtreatment to create an air gap between the lower electrode and the substrate. This is a so-called film bulk acoustic resonator (FBAR). Another method is to use a structure mounted on the substrate which houses an acoustic reflector fixed between the resonator and the substrate, which serves to prevent any acoustic interaction of the active zone of the resonator with the substrate. Figure 1 shows such a resonator design, called a solidly mounted resonator-bulk acoustic wave (SMR-BAW). The key parameters of the SMR-BAW resonator that characterize its quality substantially depend on the design of the acoustic reflector.

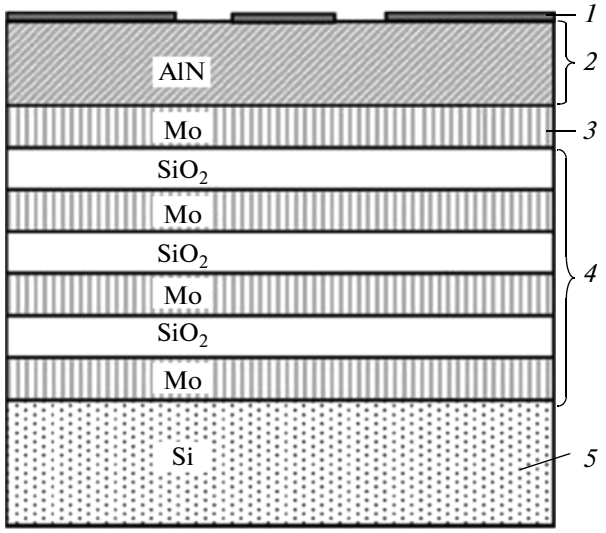

Fig. 1. SMR-BAW resonator. (*1*) upper electrode, (*2*) piezoplate, (*3*) lower electrode, (*4*) acoustic reflector, (*5*) substrate.

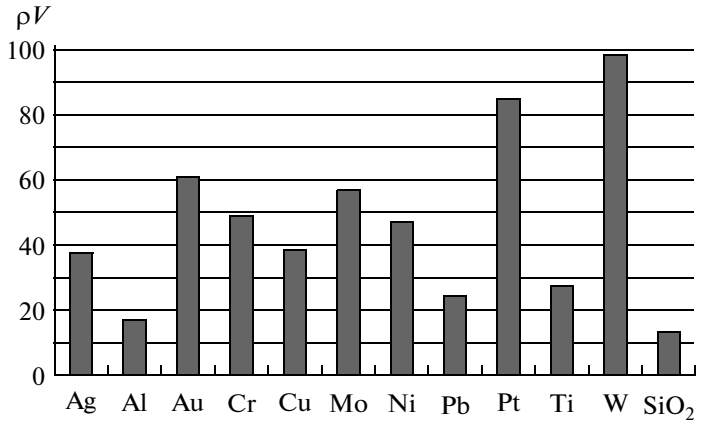

Fig. 2. The acoustic impedance $Z_a = \rho V$ for some materials.

RESONATOR WITH A QUARTER-WAVE BRAGG REFLECTOR

As a rule, SMR-BAW resonators are designed using a Bragg-type acoustic resonator [12]. The Bragg reflector provides effective localization of the longitudinal oscillation mode in the piezoactive layer material. It is a multilayer periodic structure consisting of n pairs of material layers with substantially different acoustic impedances $Z_a = \rho V$ (per surface unit), where ρ is the density of the material layer, V is the velocity of the longitudinal BAW, and the thickness of each layer is $\lambda/4$, where λ is the length of the longitudinal BAW in the layer material.

If the layer thickness is equal to a quarter-wavelength, the phase of the reflected wave differs from the phase of the incident wave by 180° after reflection from the lower surface of the first layer in the Bragg reflector. Interference of the incident and reflected waves is accomplished by the first Bragg layer (and then each successive layer) with a mirror which reflects the acoustic energy back to the resonator.

The Bragg reflector stack operates by reflecting some portion of the acoustic energy of longitudinal oscillations back to the resonator at each layer interface. The more pronounced the differences in the acoustic properties of the pair layers, the more efficient the reflection at the layer interfaces and the smaller the number of pairs in the reflector. Figure 2 shows the acoustic impedances Z_a of some materials that can be used in designing the Bragg reflector.

It follows from Fig. 2 that from the standpoint of the ratio of impedances Z_a, the following material pairs are optimal for the Bragg acoustic reflector: SiO_2/W, SiO_2/Pt, SiO_2/Mo, SiO_2/Ni.

The central operating of the SMR-BAW resonator is estimated from the elementary ratio $f = V/(2h)$, where V is the velocity of the longitudinal BAW along the direction perpendicular to the surface of the piezoactive layer from (0001) AlN (for AlN, $V \sim 11$ km/s), and h is the layer thickness. At thicknesses of the (0001)AlN layer on the order of 0.2–2 μm, the operating frequency range of such a resonator is 2–12 GHz. In the general case, the central resonator frequency f depends not only on the thickness of the AlN layer but also on the thickness and type of material of the upper and lower electrodes (Al, Ti, Mo, Ni, W, Au); it can be estimated with the help of the modified Nowotny–Benes theory [13]. This theory is based on the rigorous solution of equations that describe wave processes in the multilayer structure the resonator is made of by using correct boundary conditions at the interfaces of all layers. This makes it possible to calculate the resonator formed by any number of arbitrarily positioned arbitrary layers.

Figure 3 shows the modulus $|Z|$ and the phase φ of the electric impedance of the SMR-BAW resonator designed to operate at a frequency of 10 GHz with a classical Bragg reflector formed by four pairs of the SiO_2/Mo layers. These quantities were calculated using technique [14]. The material constants for AlN, Mo, SiO_2 required for calculations were taken from [15, 16].

The minimum of the impedance $|Z|$ corresponds to the resonance frequency (the resonance frequency of the series) $f_s = 10$ GHz; for this, the thicknesses of the active zone of the resonator were selected as follows: the thickness of the upper Mo electrode was 0.05 μm, the thickness of the (0001)AlN layer was 0.26 μm, and the thickness of the lower Mo electrode was 0.06 μm. The thicknesses of the layers in the Bragg resonator are as follows: 0.15 μm of the SiO_2 layer (the velocity of the longitudinal BAW is 5.969 km/s) and 0.17 μm of the Mo layer (the velocity of the longitudinal BAW is 6.66 km/s), which makes a quarter-wavelength at 10 GHz. The impedance maximum corresponds to the antiresonance frequency f_p (the parallel resonance frequency).

The resonance and antiresonance frequencies determine the effective resonator electromechanical coupling coefficient K_{eff}^2 [1]:

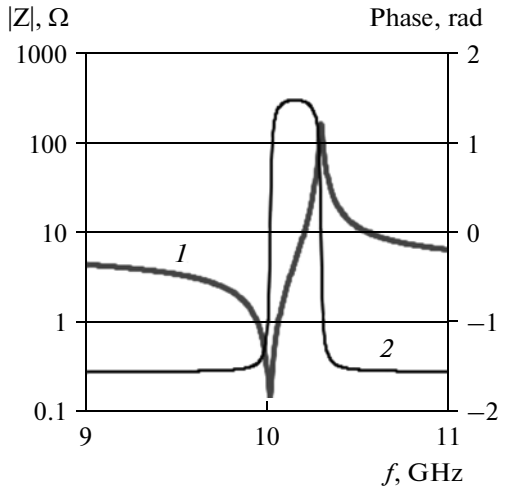

Fig. 3. Dependences of modulus $|Z|$ (curve *1*) and phase φ (curve *2*) of resonator electrical impedance on frequency f.

$$K_{eff}^2 = \frac{\pi}{2}\frac{f_s}{f_p}\left[\mathrm{tg}\left(\frac{\pi}{2}\frac{f_s}{f_p}\right)\right]^{-1} \approx \left(\frac{\pi}{2}\right)^2 \frac{f_s}{f_p}\frac{f_p - f_s}{f_p}.$$

Here, $K_{eff}^2 = 6.6\%$.

The rigorous Nowotny–Benes theory used in this case allows calculating not only the electric properties of the resonator but also the spatial distribution of all quantities (namely, three components of mechanical displacements, three normal components of the strain tensor, a normal component of the electric-flux density, and the electrical potential). In particular, Fig. 4 plots the calculated dependences of the component of longitudinal $|\,|u_1|$ and transverse $|\,|u_2|$ depth displacements for the analyzed SMR-BAW resonator.

The curves in Fig. 4 show that the Bragg reflector consisting of four pairs of SiO_2/Mo layers provides acceptable suppression of acoustic interaction of the resonator with the substrate for longitudinal wave displacement; however, it does not hinder the arrival of the wave with the transverse (shear) displacement component to the substrate.

One of the most important parameters of SMR-BAW resonators is the FOM (figure of merit)quality index, determined as [10]

$$\mathrm{FOM} = K_{eff}^2 Q.$$

Here, K_{eff}^2 is the effective electromechanical coupling coefficient, and Q is the resonator Q-factor. The larger the FOM, the higher the resonator quality.

When developing bandpass filters based on SMR-BAW resonators it is desirable to ensure three things: the effective electromechanical coupling coefficient K_{eff}^2, a high Q-factor, and the absence of parasitic resonances [10]. The coupling coefficient K_{eff}^2 is directly associated with the accessible width of the filter band and filter insertion losses. The Q-factor mainly affects

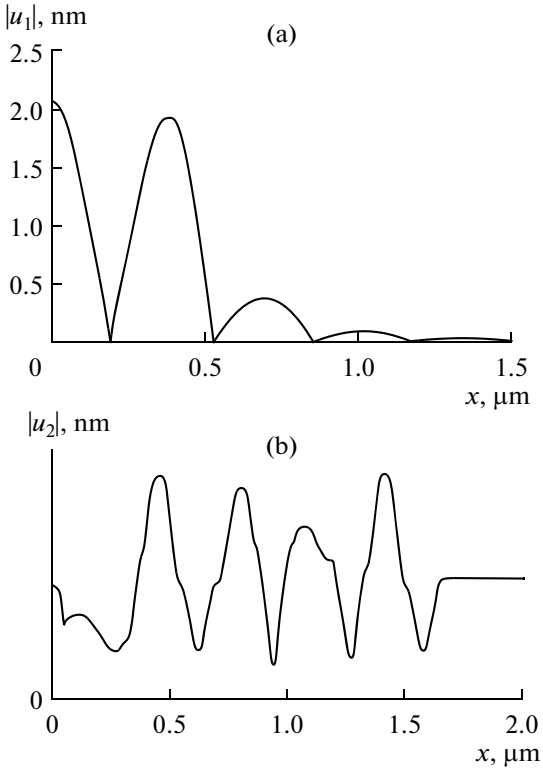

Fig. 4. Modulus of longitudinal (a) and transverse (b) displacement components as a function of the x coordinate perpendicular to layer surfaces for SMR-BAW resonator operating at 10 GHz with Bragg reflector from four alternating pairs of SiO_2 and Mo layers.

the insertion losses and the steepness of the filter band edges. Parasitic resonances in the vicinity of the main resonance of the device yield an increase in insertion losses in the filter passband.

The effective electromechanical coupling coefficient K_{eff}^2 depends on the quality of the (0001)AlN active layer (from the standpoint of its piezoproperties) and on the ratio of the electrode and piezolayer thicknesses. Traditional explanations for the mechanisms of Q-factor limitation are related either to viscous losses in the material and energy side leaks or with scattering at surface roughnesses. All these mechanisms do exist. The mechanism of Q-factor limitation in the SMR-BAW resonator owing to losses that appear due to shear BAWs was studied in [17]. Theoretically, the shear components of mechanical displacements in a BAW should be absent in the case of the used orientation of the AlN film. However, they can appear in a real structure owing to edge effects near the resonator boundary regions, microroughnesses on the surfaces, and their nonideal parallelism. As a result, some energy is transferred to these shear waves, which can substantially deteriorate the total Q-factor of the resonator.

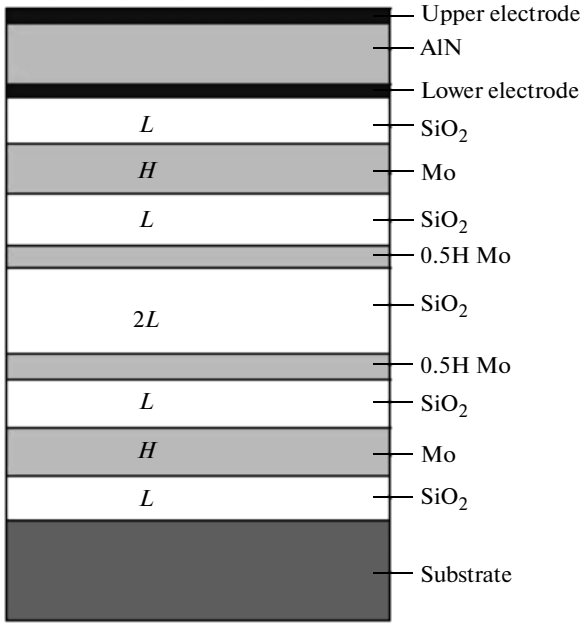

Fig. 5. SMR-BAW resonator with asymmetric reflector.

It was shown in [17] that damping of the longitudinal BAW due to the Bragg reflector at an operating frequency of 1859 MHz is 40 dB. Damping of the shear wave for the Bragg reflector is only 5 dB. If nearly 1% of the total energy is transferred to the shear wave energy, the total Q-factor of the resonator can decrease by an order of magnitude.

The resonator Q-factor can be calculated from the general definition [17]:

$$Q = E_{tot}/\Delta E_{tot},$$

where the total energy E_{tot} is assumed to consist of energies related to the longitudinal and shear waves $E_{tot} = E_{long} + E_{shear}$. Analogously, the total losses in the system are assumed to consist of the energies of losses of longitudinal and shear waves that pass through the reflector, $\Delta E_{tot} = \Delta E_{long} + \Delta E_{shear}$. Thus, it follows that

$$\frac{1}{Q} = \left(\frac{E_{long}}{E_{tot}}\right)\frac{1}{Q_{long}} + \left(\frac{E_{shear}}{E_{tot}}\right)\frac{1}{Q_{shear}},$$

where $Q_{long}$and Q_{shear} are the Q-factors that depend on the energy losses of longitudinal and shear oscillations.

In this case, the design of the acoustic reflector substantially affects trapping of the energy of both the longitudinal and the shear waves. The quarter-wave Bragg reflector efficiently reflects longitudinal BAWs, while shear BAWs are not reflected (see Fig. 4). The reason is as follows: the shear wave velocity in the majority of materials is equal, as a rule, to half the longitudinal wave velocity. Thus, the shear wave mirror represents $\lambda/2$ layers and, thus, the greater part of the shear wave energy passes freely through such layers.

RESONATOR WITH AN ASYMMETRIC REFLECTOR

An acoustic reflector whose layer thicknesses were selected using a law more complicated than the quarter-wave law was proposed in [18] to provide acoustic insulation of the shear wave. The law of distribution of reflector layer thicknesses was established based on the requirement that the reflector should provide similar effective damping of both longitudinal and shear waves. Figure 5 shows the design of a resonator with an asymmetric acoustic reflector with an (LHL) (0.5H 2L 0.5H) (LHL) structure, where L (Low) and H (High) are layers with low and high acoustic impedance Z_a.

If we denote the thicknesses of the L and H layers as t_L and t_H, respectively, then, according to [18], we have

$$t_L = \frac{\lambda_L}{2(1+c)},\ t_H = \frac{\lambda_H}{1+c},$$

where

$$c = 0.5\left(\frac{v_{Llong}}{v_{Lshear}} + \frac{v_{Hlong}}{v_{Hshear}}\right).$$

In these expressions, λ_L and λ_H are the lengths of longitudinal BAWs in the L and H layers, respectively, v_{Llong} and v_{Hlong} are the velocities of the longitudinal BAW in the L and H layers, respectively, and v_{Lshear} and v_{Hshear} are the velocities of the shear BAW in the L and H layers.

In our case, SiO_2 was taken as the material with low acoustic impedance (L layer), while Mo served as the material with high acoustic impedance (the H layer). We used a version of material constants providing the following velocities: v_{Llong} = 5969 m/s, v_{Lshear} = 3763 m/s (for SiO_2), and v_{Hlong} = 6660 m/s, v_{Hshear} = 3501 m/s (for Mo).

In accordance with the above formulas, the SMR-BAW resonator was calculated for a resonance frequency of 10 GHz using technique [14]. In the one-dimensional theory [13], the shear wave is absent for the used AlN orientation; therefore, the amplitude-frequency characteristic of the resonator with an asymmetric reflector is almost the same as that for the resonator with a quarter-wave reflector (see Fig. 3). It is necessary to keep in mind that the quarter-wave resonator does not shift the resonance frequency of the resonator that is formed only by three layers, namely, the AlN layer and two electrodes (a membrane resonator). Therefore, the resonator and reflector can easily be calculated separately. An asymmetric resonator slightly shifts the resonator resonance frequency (in our case, upwards), and as a result, the structure should be calculated as a whole. First, the reflector is calculated using the formulas of [18]; then the resonance frequency of the entire system is "adjusted" by selecting the thickness of the AlN layer and/or electrodes. In the result of this procedure the following thicknesses of the resonator and reflector layers which provide the amplitude–frequency characteristic that

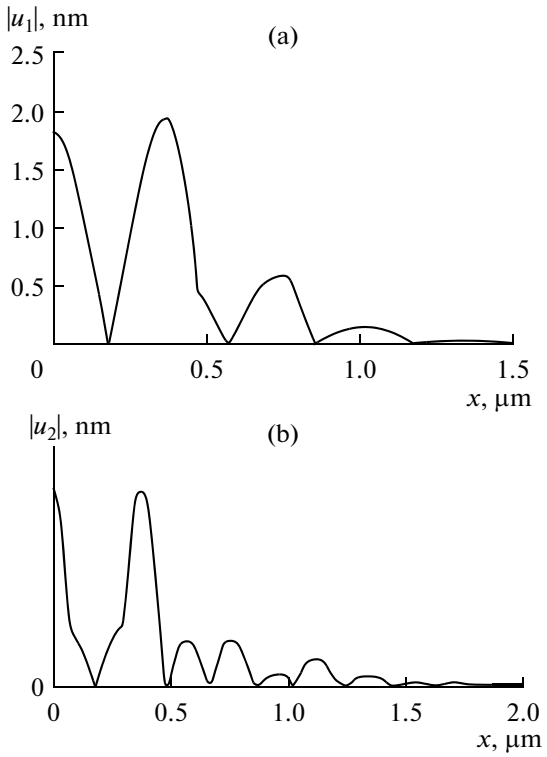

Fig. 6. Modulus of longitudinal (a) and transverse (b) displacement components as a function of the x coordinate perpendicular to layer surfaces for SMR-BAW resonator operating at 10 GHz with asymmetric reflector.

almost coincided with that shown in Fig. 3 was obtained. The thickness of the (0001)AlN film was 0.22 μm, the thickness of the upper Mo electrode was 0.0686 μm (fine frequency adjustment), and the thickness of the lower Mo electrode was 0.07 μm. The thicknesses of the L and H layers in the acoustic reflector were $t_L = 0.11$ μm and $t_H = 0.24$ μm.

The acoustic properties of the asymmetric reflector are illustrated by the curves in Fig. 6, which plots the calculated dependences of the modulus of the longitudinal and shear displacement $|u_1|$ and $|u_2|$ on the x coordinate deep into the structure.

These dependences show that the asymmetric acoustic reflector provides acceptable suppression of the resonator acoustic interaction with the substrate both for longitudinal and shear oscillation (cf. Fig, 4).

EXPERIMENT

The experimental model of the SRM-BAW resonator with an asymmetric reflector was fabricated based on the calculation data. The area of the resonator electrodes was 0.01 mm^2. A micrograph of the transverse section of the resonator layers in shown in Fig. 7. The resonator was fabricated using the techniques described in [19].

Figure 8 plots the experimentally measured frequency dependences of modulus $|Z|$ and phase φ of the electrical impedance for the fabricated SMR-BAW resonator model.

Comparison of these dependences with the calculated ones (Fig. 3) reveals that the agreement between them in not quite satisfactory. First, a frequency shift is observed. Second, there are some quantitative and qualitative divergences. The frequency shift is explained by the inevitable technological error in the formation of the thicknesses of all layers. Within this error, the following thicknesses can be obtained in the calculation process: 0.073 μm for the upper Mo electrode, 0.23 μm for AlN, 0.07 μm for the lower Mo electrode, $t_L = 0.1$ μm, and $t_H = 0.28$ μm. The antiresonance (and resonance) frequencies for these thicknesses will shift downwards and become equal to ~9.92 GHz, which almost coincides with the corresponding experimental values of 9.9 GHz (see Fig. 8a). However, the quantitative and qualitative differences of the experimental and calculation curves will remain. The curves in Fig. 3 will simply shift downwards in frequency, their shapes remaining unchanged.

These differences are attributed to the parasitic active and reactive elements that are always present in

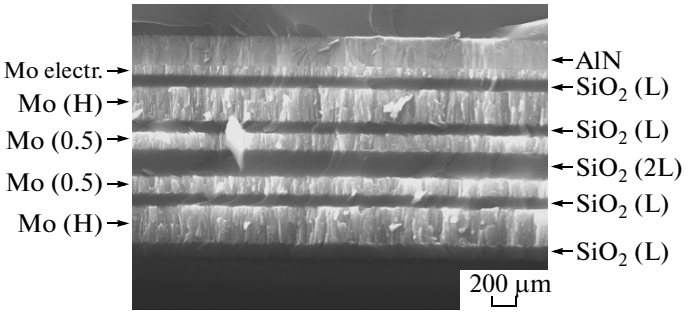

Fig. 7. Microphotograph of transverse section of multilayer structure of SMR-BAW resonator.

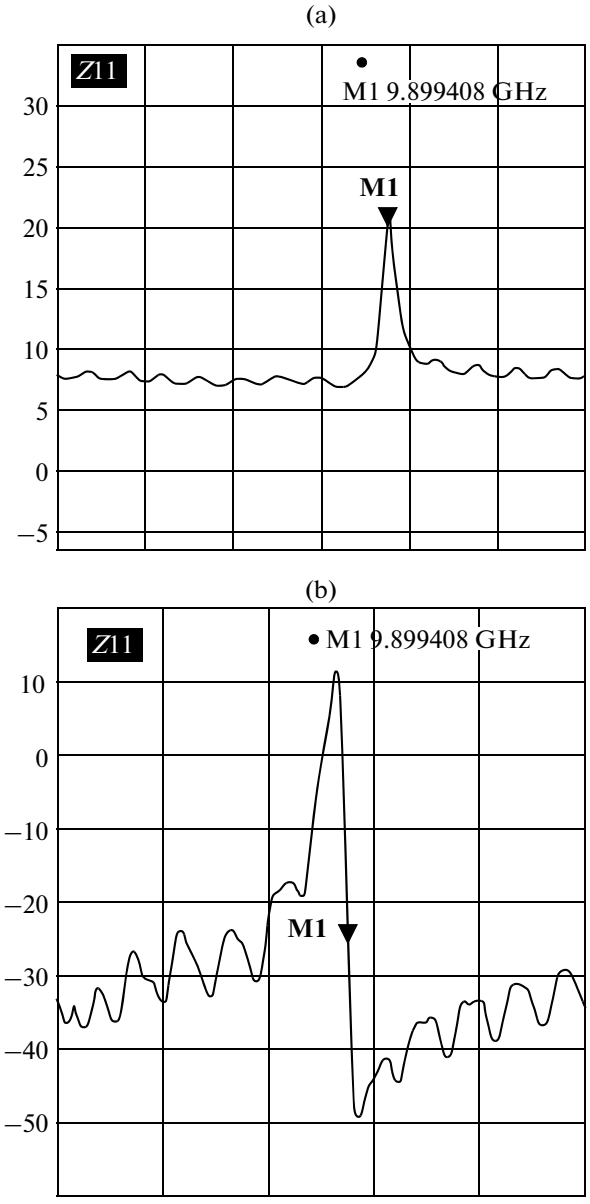

Fig. 8. Experimental frequency dependences of modulus (a) and phase (b) of electrical impedance.

any real structure and to the possible excitation of parasitic waves which propagate parallel to the layer surface (Lamb waves). All these factors cannot be taken into account within the theory that describes wave processes in the resonator layers. This theory takes into account only the properties of the layers themselves, namely, elastic, piezoelectric, dielectric, and dissipative. The latter are taken into account by adding a small imaginary part to the material constants, which simulates acoustic losses in the layer materials. It is most convenient to add the imaginary part to the material density, since any material (piezoelectric, dielectric, metal) has a nonzero isotropic density that cannot be said about other material constants (in the general case, tensor ones). The ratio of the imaginary density part to its real part can be set as $1/Q_{mech}$, where Q_{mech} is the mechanical Q-factor of the material. In this study, the following magnitudes were used: $Q_{mech} = 1500$ for AlN, $Q_{mech} = 500$ for Mo, and $Q_{mech} = 1000$ for SiO_2. These magnitudes determine the Q-factor of the entire resonator. For example, the calculated Q-factor of a membrane resonator with zero-thickness electrodes is 1500. The presence of Mo electrodes with finite thickness reduces this Q-factor; however, it cannot make it smaller than 500 (1000 for SiO_2 layers). The experimental Q-factor of the resonator is substantially lower, and this cannot be taken into account within the wave theory, which describes the processes only in the resonator layers. Parasitic elements of the structure cannot be introduced into the wave equations; however, they can be easily taken into account with the help of the modified Butterworth–Van Dyke (BvD) model [20]. The basic BvD model represents an equivalent electric circuit that includes a series LCR circuit with the capacitance C_0 connected in parallel. The series LCR circuit includes an equivalent dynamic capacitance C_m, the equivalent dynamic inductance L_m, and the equivalent dynamic resistance R_m. The quantities C_m and L_m determine the resonance frequency of the resonator; R_m, the acoustic losses in the resonator layers. All these three quantities are equivalent and cannot be determined in the framework of the BvD model itself. They can be estimated only by comparing the amplitude–frequency characteristic of this model with an analogous characteristic obtained from experiment or with the help of a rigorous theory. The quantity C_0 represents static capacitance of the capacitor formed by the electrodes and the layer (layer) between them. This is a real quantity that can be calculated and measured experimentally. The value of C_0 determines the resonance frequency of the resonator. The basic BvD model also describes the processes only in the resonator layers. The advantage of this model is related to the fact that any parasitic elements (active, reactive, parallel, series ones) in any combination can easily be connected to the equivalent circuit of the basic model. Different versions of such circuits can be found in the literature. In the literature, the basic model with the related parasitic elements is called the modified BvD model. The equivalent circuit of the modified BvD model used in our study is shown in Fig. 9.

Here, C_p is the circuit capacitance, which shunts the specific gap of the resonator, and R_s is the ohmic resistance of the electrodes and the entrance paths. Resistance R can be simulated both as real shunting ohmic losses due imperfections of mounting and acoustic losses due to excitation and propagation of parasitic waves along the resonator surface (Lamb waves). Capacitance C can include the capacitance of the elements of structural placement and/or the measuring circuit, as well as the reactive properties of parasitic waves.

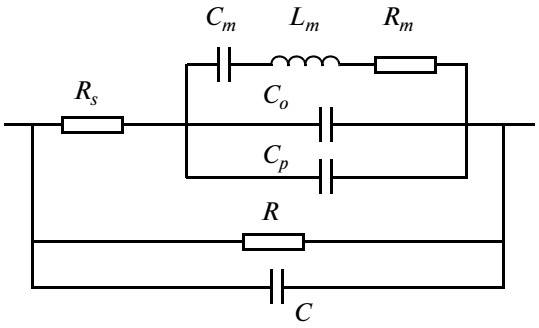

Fig. 9. Equivalent circuit of modified BvD model used in this study.

Elements C_m, L_m, and R_m of the equivalent circuit in the basic BvD model can be determined unambiguously by comparing the amplitude-frequency characteristic of this circuit with the characteristic calculated using the rigorous theory [13]. Static capacitance C_0 is calculated based on the geometrical dimensions and dielectric properties of the resonator active zone. For the analyzed resonator, the following values were obtained:

$$C_m = 0.191 \text{ pF}, L_m = 0.00141 \text{ μH},$$
$$R_m = 0.159 \text{ Ω}, C_0 = 3.657 \text{ pF}.$$

The parasitic element of the equivalent circuit cannot be calculated at all. Moreover, there are no methods for measuring them or experimentally separating them one from another. They can be only selected based on the condition of maximum closeness of calculation and experimental results. It is possible to simultaneously vary (increase) R_m to simulate additional acoustic losses in resonator layers due to technological imperfection. In this case, the following values were obtained:

$$R_m = 0.24 \text{ Ω}, R_s = 8.8 \text{ Ω},$$
$$C_p = 0.5 \text{ pF}, R = 35 \text{ Ω}, C = 0.43 \text{ pF}.$$

The calculated dependence of the resonator impedance for the frequency obtained for the equivalent circuit of the modified BvD model is shown for these values in Fig. 10.

These dependences are almost identical to the experimentally obtained ones (see Fig. 8). The frequency of the parallel resonance is 9.9 GHz.

Based on the steepness of the φ(*f*) curve, it is possible to estimate the Q-factor of the resonator at the parallel resonance frequency f_p [12]:

$$Q_p = \frac{1}{2} f_p \left| \frac{d\varphi}{df} \right|_{f_p},$$

where φ is the phase of impedance Z in radians.

The thus-obtained Q-factor of the resonator was $Q_p = 150$. The calculated dependences give an estimate of the same order of magnitude.

The obtained experimental value of the effective electromechanical coupling coefficient was $K_{eff}^2 =$

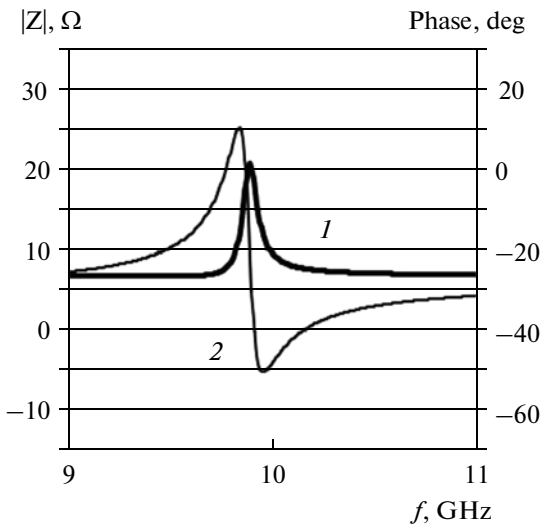

Fig. 10. Calculated frequency dependences of modulus (curve *1*) and phase (curve *2*) of resonator impedance obtained in joint application of rigorous theory and modified BvD model.

5.2% (calculation performed with the modified BvD model gives $K_{eff}^2 = 5.37\%$).

Thus, joint application of the rigorous Nowotny–Benes theory and the modified BvD model makes it possible to obtain theoretical calculation results that almost coincide with the experimental results obtained for the resonator model fabricated based on calculation data. In addition, the BvD model allows studying the specific reasons for the change in the parameters of a real resonator compared to the calculated parameters obtained with the rigorous theory. In particular, it can immediately seem that the high ohmic resistance of the electrodes and input paths R_s drastically reduces the Q-factor at the series resonance frequency, but it does not affect the parallel resonance. The Q-factor at the parallel resonance frequency decreases mainly due to additional acoustic losses that appear in the layers in the result of technological imperfections (surface roughness of nonideal parallelism) or energy losses in the transverse direction due to excitation and propagation of parasitic Lamb waves. Additional losses inside layers are simulated by increasing the equivalent dynamic resistance R_m; losses due to parasitic waves, by increasing resistance R.

The shunting parasitic capacitance C_p results in a decrease in the antiresonance frequency f_p and, thus, a reduction in the effective electromagnetic coupling coefficient K_{eff}^2. However, capacitance C_p does not affect the series resonance frequency.

Finally, capacitance C, which shunts the entire circuit, mainly results in a general shift of the impedance phase curve downwards toward negative values. Without this capacitance, the phase curve beyond the reso-

nances should be in the vicinity of zero. The presence of this capacitance can be attributed to peculiarities in the structural mounting, elements of the measuring setup, and reactive properties of transverse parasitic waves.

CONCLUSIONS

The entire history of acoustoelectronics as an important scientific and applied interdisciplinary field [21, 22] points to the following key tendencies: application of new types of waves and physical phenomena to develop and upgrade electroacoustic devices and improve their characteristics by using new materials and technologies. In particular, the tendency toward increasing the frequencies and miniaturization of elements of acoustic and radioelectronic devices related to it is of particular importance. The development of miniature and high-frequency elements opens new fields of application and increases the density of the processed data flows.

This study is devoted to the problems of transition to the frequency range from units to tens of GHz. This gives rise to new physical and engineering problems, some of which were discussed above. A numerical analysis is presented of the key parameters of the SMR-BAW resonator based on the piezoelectric thin (0001)AlN film with different types of acoustic resonator designed to operate at 10 GHz. A prototype of the SMR-BAW resonator with an asymmetric acoustic reflector was developed, and the results of an experimental study of the resonator parameters are given. Comparative analysis of theoretical calculation of the resonator parameters and the experimentally obtained data was performed using the Nowotny–Benes theory and the modified Butterworth–Van Dyke model. The results of the analysis revealed the reasons why the Q-factor of the resonator was affected.

ACKNOWLEDGMENTS

The study was supported in part by a grant of the RF Government for rendering assistance to the scientific research carried our under the supervision of leading scientists in Russian educational institutions for higher professional training (Nizhni Novgorod State University, project no. 11.G34.31.0066).

REFERENCES

1. I. Ya. Ashbel', M. Yu. Dvoesherstov, and S. G. Petrov, Akust. Zh. **36**, 360 (1990).
2. M. Yu. Dvoesherstov, S. G. Petrov, V. I. Cherednik, and A. P. Chirimanov, Acoust. Phys. **47**, 415 (2001).
3. M. Yu. Dvoesherstov, V. A. Savin, and V. I. Cherednik, Acoust. Phys. **47**, 682 (2001).
4. M. Yu. Dvoesherstov, V. I. Cherednik, A. P. Chirimanov, and S. G. Petrov, Acoust. Phys. **48**, 678 (2002).
5. M. Yu. Dvoesherstov, V. I. Cherednik, and A. P. Chirimanov, Acoust. Phys. **50**, 512 (2004).
6. M. Yu. Dvoesherstov, V. I. Cherednik, S. G. Petrov, and A. P. Chirimanov, Acoust. Phys. **50**, 670 (2004).
7. V. I. Cherednik and M. Yu. Dvoesherstov, Acoust. Phys. **51**, 469 (2005).
8. V. I. Cherednik and M. Yu. Dvoesherstov, Acoust. Phys. **56**, 37 (2010).
9. G. Wingqvist, J. Bjurström, and I. Katardjiev, *Proc. IEEE Ultrasonics Symposium*, 50 (2005).
10. R. Rich and S. Jose, *Proc. IEEE Ultrasonics Symposium*, 1029 (2007).
11. K. M. Lakin, IEEE Microwave Mag. **4**, 61 (2003).
12. M. Allah, R. Thalhammer, J. Kaitila, et al., A Solid-State Electronics **54**, 1041 (2010).
13. H. Nowotny and E. Benes, J. Acoust. Soc. Am. **82**, 513 (1987).
14. V. I. Cherednick and M. Y. Dvoesherstov, in *Waves in Fluids and Solids* Ed. by R. P. Vila, Chap. 3, p. 69 (2011).
15. G. Carlotti, F. Hickernell, M. Liaw, and L. Palmiergi, *Proc. IEEE Ultrasonics Symposium* 53 (1995).
16. S. Ballandras, E. Gavignet, E. Bigler, and E. Henry, Appl. Phys. Lett. **71**, 1625 (1997).
17. S. Marksteiner, J. Kaitila, G. Fattinger, and R. Aigner, *Proc. IEEE Ultrasonics Symposium* 329 (2005).
18. S. Jose, A. Jansman, and R. Hueting, *Proc. Int. Ultrasonics Symposium* 2111 (2009).
19. A. P. Sidorin, A. V. Belyaev, M. Yu. Dvoesherstov, and S. E. Korshunov, *Proc. Sci. Conf. Sci. Counsel Russ. Acad. Sci. Sess. on Acoustics and 25th Sess. Russ. Acoust. Soc.*, Taganrog, vol. 1, 288 (2012).
20. P. D. Bradley, S. Wartenberg, and R. C. Ruby, *Proc. IEEE Ultrasonics Symposium*, 53 (2000).
21. Yu. V. Gulyaev and F. S. Khikernell, Acoust. Phys. **51**, 81 (2005).
22. G. S. Kino, *Acoustic Waves: Devices, Imaging, and Analog Signal Processing* Prentice-Hall, Englewood Cliffs, NJ, USA (1987).
23. G. S. Kino, Acoustic Waves: Devices, Imaging, and Analog Signal Processing. Prentice-Hall, Englewood Cliffs, NJ, USA (1987).

Translated by L. Borodina